International Journal of New Horizons in Physics

http://dx.doi.org/10.18576/ijnhp/030204

Study Some Physical Properties of the Semiconducting P_2O_5 - V_2O_5 - As_2O_3 -Fe_2O_3 Oxide Glasses

M. Shapaan[*]

Phys. Dept., Faculty of Science, Al-Azhar Univ., Nasr City, Cairo 11884, Egypt.

Received: 21 Feb. 2016, Revised: 22 Mar. 2016, Accepted: 24 Mar. 2016.
Published online: 1 Jul. 2016.

Abstract: Oxide glasses with composition $35P_2O_5$ $(45\text{-}x)V_2O_5$ xAs_2O_3 $20Fe_2O_3$ $(0 \le x \le 25$ mol %) have been prepared by the conventional melt quenching technique. The glassy state of the as prepared samples is characterized using X-ray diffraction (XRD) and differential thermal analysis (DTA). In order to understand the effect of As_2O_3 contents on the structure and the structural changes occurring in these glasses, the density, ρ, and molar volume, V_m, measurements have also been made. The density increases and molar volume decreases with increasing As_2O_3 contents. The dc conductivity decreases with increasing As_2O_3 contents. The room temperature dc conductivity is typically 10^{-5} - 10^{-9} (Scm^{-1}) with activation energy 0.28 - 0.49 (eV). Two glass transition temperatures, T_{g1} and T_{g2}, are detected at the DTA traces of the investigated glass system. From the dependence on heating rates of, T_{g1}, T_{g2}, and T_p, the activation energies for glass transitions, E_{g1}, E_{g2}, and the activation energy for crystallization, E_c, are calculated. All the results confirmed that, the thermal stability increases with increasing As_2O_3 contents in the investigated glass system. The glass sample with x = 25 (mol %) is of the highest glass thermal stability $\Delta T_x = 207 \pm 2$ (K) at 20 (K/min) heating rate and crystallization activation energy $E_c = 224.5 \pm 3$ (kJ/ mol).

Keywords: Amorphous semiconductors; Oxide glasses; Conductivity; Thermal stability; Glass transition temperature

1 Introduction

Oxide glasses are of special scientific and technological interest because of their application in various industrial fields. From previous studies it was found that, phosphate glasses have low glass transition temperatures, large thermal expansion coefficients and glass formation takes place over a wide composition range [1, 2].

The most important class of phosphate based glasses is the one which containing transition metal oxides such as Fe_2O_3 and V_2O_5 as an example [3].

Recent studies of phosphate glasses have shown that the addition of iron has a significant effect on the glass transition temperature, the thermal expansion coefficient and the chemical durability [4, 5].

Also it was found that the chemical durability increases dramatically with the addition of Fe_2O_3 into phosphate glasses and this changes may be attributed to the replacement of the P-O-P bonds by more chemically durable P-O-Fe^{2+} and/or P-O-Fe^{3+} bonds [6-8]. At the same time studies have shown that, the formation of P-O-Fe bonds are responsible for the formation of small polarons and as a result the electric conduction in these glasses occurs by thermally activated small polaron hopping from the low valance state Fe^{2+} (Ferrous ions) to the high valance state Fe^{3+} (Ferric ions) [7].

For vanadium phosphate glasses the same conduction mechanism was found also, where the electric conduction in these glasses may be due to small polarons hopping (SPH) which occurs from V^{4+} sites to the neighboring V^{5+} sites [8-11].

The present work aims to study the effect of partial replacement of V_2O_5 by As_2O_3 on the structure, electric conduction, thermal stability and crystallization kinetics of the as quenched semiconducting $35P_2O_5$ $(45\text{-}x)V_2O_5$ xAs_2O_3 $20Fe_2O_3$ (x = 0, 5, 10, 15, 20 and 25 mol %) glass system.

2 Materials and methods

2.1 Glasses preparation

The glass samples having the general chemical formula $35P_2O_5$ (45-x)V_2O_5 xAs_2O_3 20Fe_2O_3 (x = 0, 5, 10, 15, 20 and 25 mol %) have been prepared by the melt quenching technique. The preparation is carried out by melting homogeneous mixtures of reagent grade $NH_4H_2PO_4$, V_2O_5, As_2O_3 and Fe_2O_3 (with purity not less than 99.8 %) in porcelain crucibles using an electric furnace at 1000 ^{0}c for 2 h. The melts are quenched between two pre-cooled copper plates to form (2cmx2cmx2mm) glass samples.

2.2 Properties measurements

The glassy states of the as-prepared samples are detected using a Philips X-ray diffractometer PW/1710 with Ni filtered, Cu Kα radiation (λ = 1.542 A˚) powered at 40 (kV) and 30 (mA).

The room temperature densities of the as prepared glass samples are measured using the suspension weight method based on the Archimedes principle using toluene as an immersion liquid whose density is (0.868 g/cm^3).

The dc conductivity (σ_{dc}) of the as-quenched glasses is measured at temperatures between 300 and 500 K and under a constant dc voltage. For electric measurements the as prepared glass samples are polished to obtain optically parallel surfaces of 1.5 (mm) thickness. In order to achieve the best electrical contact between the glass samples and the electrodes of the sample holder the measurements are carried out on the silver paste coated pellets. The value of the current at different temperatures is measured using a Picoammeter (Keithley 485 Autoranging Picoammeter) and the *I-V* characteristic between electrodes is verified.

The calorimetric measurements are carried out using differential thermal analysis Shimadzu (50) with an accuracy of ± 0.1 (K). For each heating rate the calorimeter is calibrated, using the well - known melting temperatures and melting enthalpies of zinc and indium supplied with the instrument. Twenty milligram powdered samples, crimped into aluminum pans, and scanned at continuous heating rates, β (= 5, 10, 15, 20 and 30 K/min). The values of the glass transition temperature, T_g, the crystallization extrapolated onset temperature, T_{cr}, and the crystallization peak temperature, T_p, are determined with accuracy ± 2 (K) by using the microprocessor of the thermal analyzer.

3 Results and Discussion

3.1 Density and Molar volume

The change in the density with composition of the investigated oxide glass system can be expressed in terms of apparent volume occupied by 1g atom of oxygen (molar volume V_m) which can be calculated from the room temperature measured density and composition using the following relation [12];

$$\mathbf{V_m = \sum(n_i M_w)/\rho} \qquad (1)$$

where, M_w, is the molecular weight of oxide, n_i, is the molar fraction and, ρ, is the density of the sample. From the density measurements of the $35P_2O_5$ (45-x)V_2O_5 xAs_2O_3 20Fe_2O_3 (x = 0, 5, 10, 15, 20 and 25 mol %) glass samples it is found that the density increases with increasing As_2O_3 contents as shown in Fig. 1(a) and this may be due to the higher molecular mass of As_2O_3 when compared to V_2O_5. The relative error in these measurements is about ± 0.01 (g/cm^3). Fig. 1(b) shows the variation of the molar volume, V_m, of the investigated glass system as a function of As_2O_3 contents. It is clear from this Figure that, the molar volume decreases with increasing As_2O_3 contents. This behavior may be attributed to the formation of As-O bonds, act to reticule the phosphate network and lead to close the network structure.

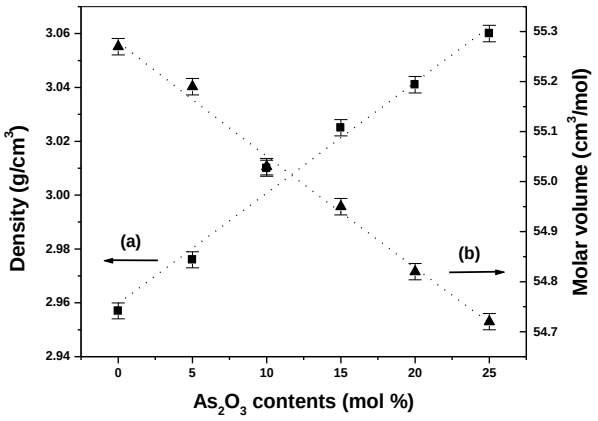

Fig. 1. Density, ρ, and molar volume, V_m, of the $35P_2O_5$ (45-x)V_2O_5 xAs_2O_3 20Fe_2O_3 (x = 0, 5, 10, 15, 20 and 25 mol %) glass system as a function of As_2O_3 contents.

The same behavior for the variation of the density, ρ, and molar volume, V_m, was found in previous articles for some oxide glasses [12-14]. The values of the measured densities and the calculated molar volumes of the investigated glass samples are listed in Table 1.

3.2 Dc conductivity measurements

The variations of the dc electrical conductivity, σ_{dc}, of the $35P_2O_5$ (45-x)V_2O_5 xAs_2O_3 20Fe_2O_3 (x = 0, 5, 10, 15, 20 and 25 mol %) glass samples as a function of temperature and As_2O_3 contents are studied in more details

(Figure 2). It is clear from this Figure that the plots $\ln\sigma_{dc}$ vs. 1/T [K^{-1}] of the investigated glass samples are linear over the temperature range 300 - 500 (K) and the temperature dependence of the dc conductivity, σ_{dc}, obeys Arrhenius relationship;

$$\sigma_{dc} = \sigma_0 \exp[-E_{dc}/k_B T] \quad (2)$$

where, E_{dc}, is the activation energy for conduction, σ_0, is the pre-exponential factor, k_B, is the Boltzmann constant and, T, is the absolute temperature in (K).

The activation energies of the investigated glass samples are determined from the slope of $\ln\sigma_{dc}$ vs. 1/T [K^{-1}]. The activation energies are then evaluated by least squares fitting method of Eq. (2). Fig. 3(a) shows the variation of the dc conductivity of the investigated glass samples as a function of As_2O_3 contents at different temperatures (303, 403 and 453 K) as an example. Fig. 3(b) shows the variation of the activation energies of the investigated glass samples as a function of As_2O_3 contents. It is found that the dc conductivity, σ_{dc}, increase with increasing temperature and decreases with increasing As_2O_3 contents. The increase of the dc conductivity with increasing temperature may be attributed to the increase of the thermally activated small polarons hopping (SPH) [15, 16] which contributed to the electric conduction. The values of, σ_{dc}, for the free As_2O_3 glass sample ($35P_2O_5$ $45V_2O_5$ $20Fe_2O_3$) are $1.14x10^{-5}$, $1.70x10^{-4}$ and $4.17x10^{-4}$ (Scm^{-1}) at temperatures 303, 403 and 453 (K) respectively (as an example).

The decreasing in the dc conductivity with the partial replacement of V_2O_5 (TMO) by As_2O_3 may be attributed to the decease of the transition metal oxide (TMO) in the composition and as a result decreasing the number of small polarons hopping (SPH) [16, 17]. The room temperature dc conductivity decreases from $1.14x10^{-5}$ to $4.01x10^{-9}$ (Scm^{-1}), and the activation energy increases monotonously from 0.28 to 0.49 ± 0.01(eV) with increasing As_2O_3 contents from 0 to 25 (mol %).

The conduction mechanism of the present amorphous semiconductor system depend mainly on the electron hopping from V^{4+} sites to the neighboring V^{5+} sites [10, 11] and the vanadium ions play the role of glass network modifier (GNM). Generally, it is known that, the decreases in the dc conductivity with decreasing vanadium oxide contents may be attributed to decrease of non-bridging oxygen. In the same time as shown in Figure 3 the decreases of the dc conductivity and increases the activation energy with increasing As_2O_3 contents may be attributed to decrease of the density of the localized states in the band gab near the Fermi level of the semiconducting glass samples. The obtained results are in good agreement with the already available results for different semiconducting glasses [18, 19]. The values of the dc conductivity at different temperatures (303, 403 and 453 K), and the activation energies of the investigated glass samples are listed in Table 1.

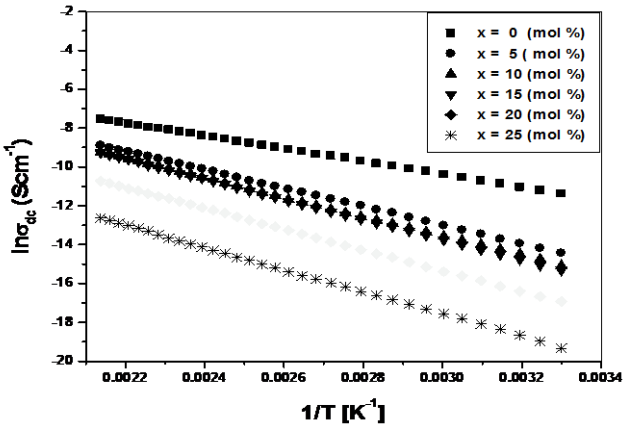

Fig. 2. Plots of $\ln(\sigma_{dc})$ vs. 1/T [K^{-1}] of the $35P_2O_5$ (45-x)V_2O_5 xAs_2O_3 $20Fe_2O_3$ (x = 0, 5, 10, 15, 20 and 25 mol %) glass system.

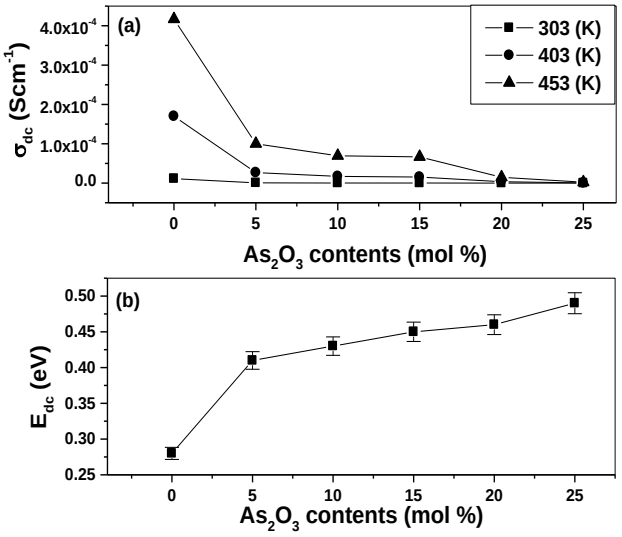

Fig. 3. (a) - Dc Conductivity as a function of As_2O_3 contents at different temperatures (303, 403 and 453 K) of the $35P_2O_5$ (45-x)V_2O_5 xAs_2O_3 $20Fe_2O_3$ (x = 0, 5, 10, 15, 20 and 25 mol %) glass system. (b) - The activation energy of the investigated glass samples as a function of As_2O_3 contents.

3.3 Thermal analysis and thermal stability of glass

All the investigated glass samples exhibit two endothermic minima, T_{g1} and T_{g2} followed by one crystallization peak temperature, T_p. The first endothermic minima represent the glass transition temperature, T_{g1},

which confirm the glassy nature of the investigated samples. The second endothermic minima, T_{g2}, may be attributed to the ferroelectric transition temperature [11]. Fig. 4 shows the DTA traces of the semiconducting $35P_2O_5$ $(45\text{-}x)V_2O_5$ xAs_2O_3 $20Fe_2O_3$ (x = 0, 10, 20 and 25 mol %) glass samples at 15 (K/min) heating rate. It is found that, the thermal transition data, T_{g1}, T_{g2}, T_{cr} and T_p, did not changed monotonously with the partial replacement of V_2O_5 by As_2O_3. Fig. 5 shows the effect of heating rate, β, on the thermal transition data for the glass sample with x = 25 (mol %) at 10 and 20 (K/min) as an example. It is found that the thermal transition data are shifted to higher temperatures with increasing the heating rate, β.

The inset of Figure 5 shows the variation of the thermal stability criteria $\Delta T_x = T_{cr} - T_g$ [20] as a function of the As_2O_3 contents. It is found that, ΔT_x increases with increasing As_2O_3 contents, this meaning that, the partial replacement of V_2O_5 by As_2O_3 contents increases the thermal stability of the investigated glass samples [21].

The increases in the super-cooled liquid region ($\Delta T_x = T_{cr} - T_g$) as a function of As_2O_3 contents may be attributed to the replacement of the weak O-V-O linkages by the strong O-As-O linkages [22, 23] indicates strengthening of the glass network as V_2O_5 is replaced by As_2O_3. The thermal transition data (T_{g1}, T_{g2}, T_{cr} and T_p) and the thermal stability criteria, ΔT_x, at 20 K/min heating rate of the investigated glass samples are listed in Table 2.

3.3.1 Glass transition analysis

The variation of the glass transition temperature, T_g, as a function of heating rate, β, can be approached by several equations. The first approach has been described using the empirical relationship suggested by Lasoka [24] which is expressed as;

$$\mathbf{T_g = A_g + B_g ln(\beta)} \qquad \mathbf{(3)}$$

where, A_g, and, B_g, are constants for a given glass composition. The value of, A_g, represents the glass transition temperature at 1(K/min) heating rate and the value of, B_g, is related to the cooling rate of the melt. Fig. 6 shows the variation of the glass transition temperatures, T_{g1}, and T_{g2}, with ln(β) for the investigated glass samples (x = 0, 10, 20 and 25 mol %). The values of, A_{g1}, B_{g1}, A_{g2} and B_{g2}, are obtained from the straight line fitting of the relation between, T_g and ln(β) (Table 2). The second approach regarding the dependence of the glass transition temperature on the heating rate is based on Kissinger's method [25]. The activation energies of enthalpy relaxation of the glass transitions, E_{g1} and E_{g2}, can be determined using Kissinger formula, which was originally derived for the crystallization process and suggested to be valid for the glass transition. This formula has the following form;

$$\mathbf{ln\left(\frac{T_g^2}{\beta}\right) = \frac{E_g}{RT_g} + const.} \qquad \mathbf{(4)}$$

where, R, is the universal gas constant, T_g, is the glass transition temperature, E_g, is the glass transition activation energy and, β, is the heating rate. The values of the glass transition activation energies, E_{g1}, and E_{g2}, can be estimated from $\ln(T_{g1}^2/\beta)$ vs. $1000/T_{g1}$ and $\ln(T_{g2}^2/\beta)$ vs. $1000/T_{g2}$ respectively as shown in Fig. 7.

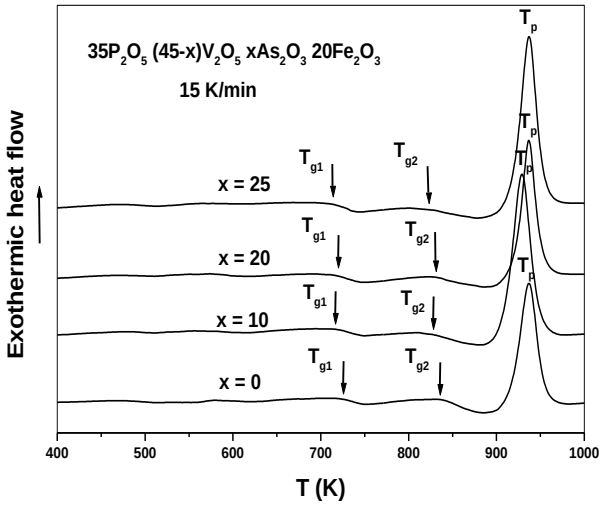

Fig. 4. Typical DTA traces of the $35P_2O_5$ $(45\text{-}x)V_2O_5x$ As_2O_3 $20Fe_2O_3$ (x = 0, 10, 20 and 25 mol %) glass samples at 15 (K/min) heating rate.

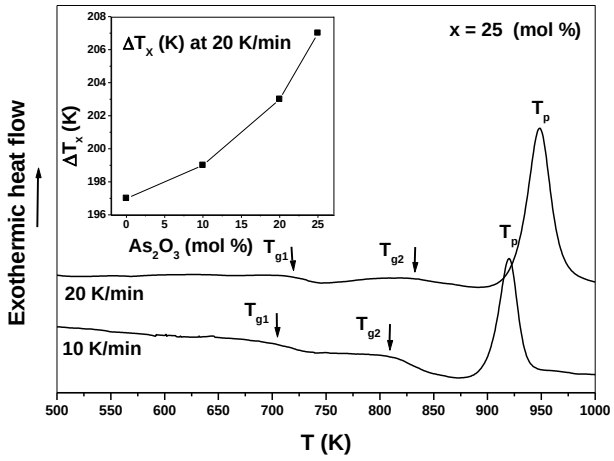

Fig. 5. Typical DTA curves of the $35P_2O_5$ $(45\text{-}x)V_2O_5$ xAs_2O_3 $20Fe_2O_3$ (x = 25 mol %) glass sample at 10 and 20 (K/min) heating rate. The inset shows $\Delta T_x = T_{cr} - T_g$ as a function of As_2O_3 contents at 20 (K/min).

The values of the glass transition activation energies,

E_{g1} and E_{g2}, are evaluated by least squares fitting method of eq. (4) and the solid lines are guides for eyes. The third approach to determine the glass transitions activation energies, E_{g1} and E_{g2}, is based on a simplified form of eq. (4). According to Mahadevan et al. [26] Kissinger's equation was simplified to the following form;

$$\ln(\beta) = -E_g/RT_g + \text{const.} \quad (5)$$

The values of the glass transition activation energies, E_{g1}, and E_{g2}, can be estimated from ln(β) vs. $1000/T_{g1}$ and ln(β) vs. $1000/T_{g2}$ as shown in Fig. 8. The values of the glass transition activation energies, E_{g1} and E_{g2}, are evaluated by least squares fitting method of eq. (5) and the solid lines are guides for eyes. The calculated activation energies by Kissinger and Mahadevan et al. analysis have nearly the same values.

Fig. 9 shows the variation of the glass transition activation energies, E_{g1} and E_{g2}, as a function of As_2O_3 contents. It is clear from this Figure that the glass sample with 10 (mol %) As_2O_3 has the highest values of, E_{g1}, and, E_{g2}, which have the following values. From Kissinger analysis, E_{g1} and E_{g2}, are equal to 280 and 296 ± 3 (kJ/mol) and from Mahadevan et al. analysis equal to 281 and 298 ± 3 (kJ/mol) respectively. The obtained values of, E_{g1}, and, E_{g2}, are listed in Table 3.

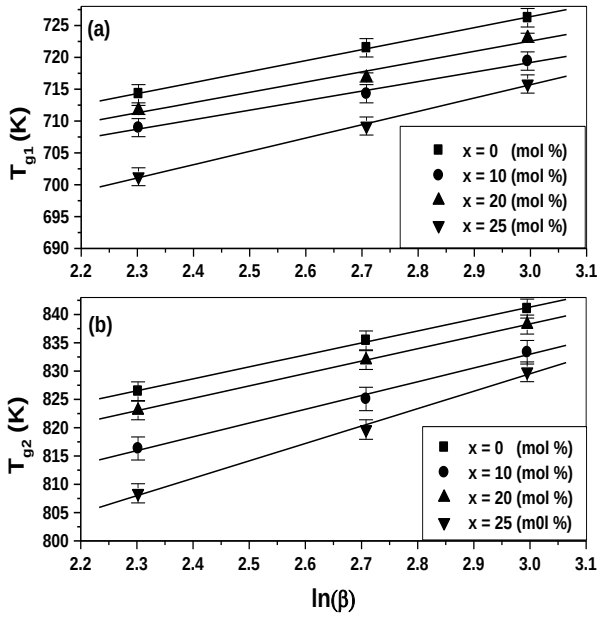

Fig. 6. The variation of the glass transition temperatures, T_{g1}, and, T_{g2}, as a function of the heating rate, β, of the as quenched $35P_2O_5$ $(45\text{-}x)V_2O_5$ xAs_2O_3 $20Fe_2O_3$ (x = 0, 10, 20 and 25 mol %) glass samples.

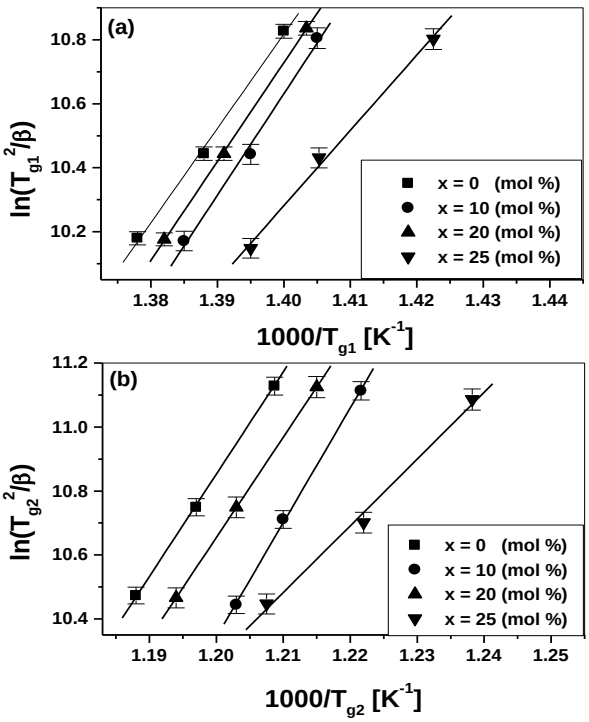

Fig. 7. Plots of (a) - $\ln(T_{g1}^2/\beta)$ vs. $1000/T_{g1}$ and (b) - $\ln(T_{g2}^2/\beta)$ vs. $1000/T_{g2}$ of the as quenched $35P_2O_5$ $(45\text{-}x)V_2O_5$ xAs_2O_3 $20Fe_2O_3$ (x = 0, 10, 20 and 25 mol %) glass samples.

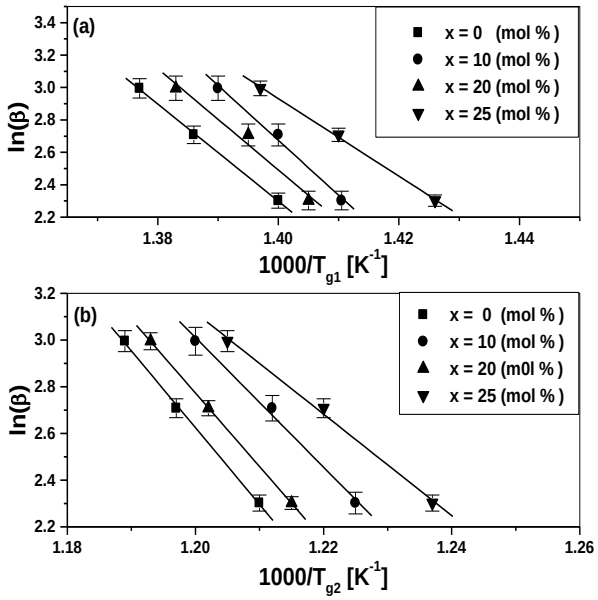

Fig. 8. Plots of (a) - ln(β) vs. $1000/T_{g1}$ and (b) - ln(β) vs. $1000/T_{g2}$ of the as quenched $35P_2O_5$ $(45\text{-}x)V_2O_5$ xAs_2O_3 $20Fe_2O_3$ (x = 0, 10, 20 and 25 mol %) glass samples.

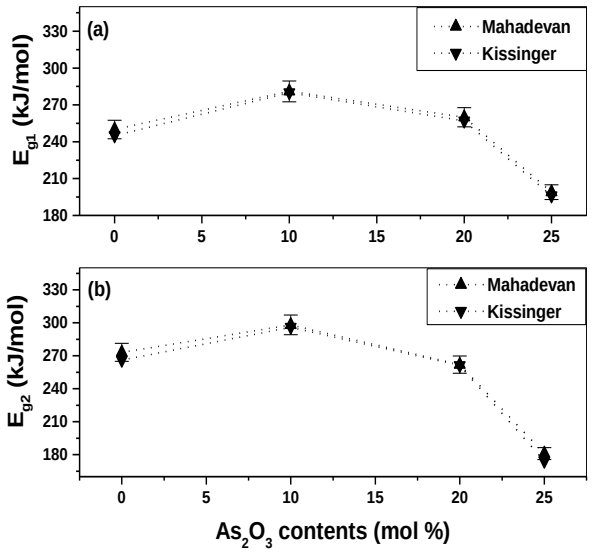

Fig. 9. Glass transition activation energies, E_{g1} and E_{g2}, as a function of As_2O_3 contents.

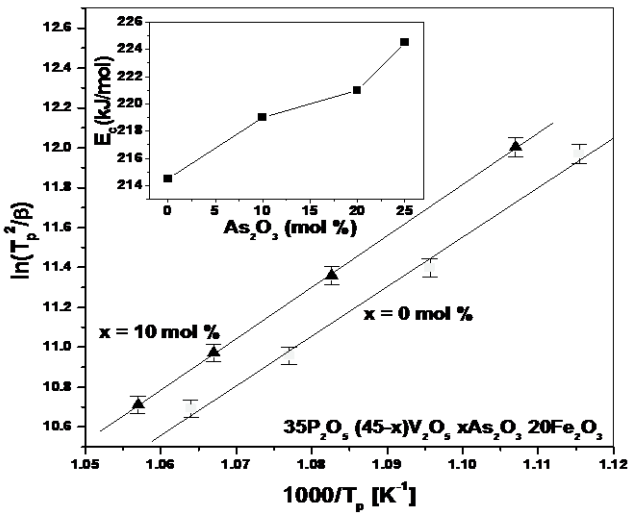

Fig. 10. Plots of $\ln(T_p^2/\beta)$ vs. $1000/T_p$ of the as quenched $35P_2O_5$ (45-x)V_2O_5 xAs_2O_3 $20Fe_2O_3$ (x = 0 and 10 mol %) glass samples. The inset shows, E_c, as a function of As_2O_3 contents.

3.3.2 Crystallization kinetics and kinetic exponent

In order to estimate the activation energy of crystallization, E_c, by using the variation of crystallization peak temperature, T_p, with, β, Vazquez et al. [27] developed the proposed method by Kissinger [25] for non-isothermal analysis of diversification as follows;

$$\ln\left(\frac{T_p^2}{\beta}\right) = \frac{E_c}{RT_p} + \ln\left(\frac{E_c}{Rk_0}\right) \qquad (6)$$

where k_0 is the frequency factor.

Fig. 10 shows the relation $\ln(T_p^2/\beta)$ vs. $1000/T_p$ of the as quenched $35P_2O_5$ (45-x)V_2O_5 xAs_2O_3 $20Fe_2O_3$ (x = 0 and 10 mol %) glass samples (as an example). From the slope of the straight line fitting of the experimental data the crystallization activation energy, E_c, is evaluated by the least squares fitting method of eq. (6) and the solid lines are guides for eyes. The inset of Fig. 10 shows the variation of the crystallization activation energy, E_c, of the as prepared glass samples as a function of As_2O_3 contents. It is clear from this Figure that, E_c, increases monotonously with increasing As_2O_3 contents. From the inset of Figure 5 and the inset of Figure 10 it is observed that the crystallization activation energy, E_c (nucleation barrier) is directly related to the width of the super-cooled liquid region (ΔT_x). This reflected that the thermal stability of the investigated glass samples increases with increasing As_2O_3 contents. The crystallization activation energy, E_c, and the frequency factor, k_0, are listed in Table 3.

The crystallization fraction, χ, can be expressed as a function of time according to the Johnson–Mehl–Avrami equation [28-30];

$$\chi(t) = 1 - \exp[-(kt)^n] \qquad (7)$$

where, n, is the Avrami exponent, which depends on the mechanism of the growth and dimensionality of crystal growth and, k, is the reaction rate constant, which is given by the following formula;

$$k = k_0 \exp(-E_c/RT) \qquad (8)$$

where, E_c, is the activation energy of crystallization, R, is the universal gas constant, T, is the isothermal temperature and, k_0, is the frequency factor. For the non-isothermal method, the theoretical basis for interpreting DTA results is provided by the formal theory of transformation kinetics, which developed by Johnson et al. [28] and Avrami [29, 30]. The fraction, χ, crystallized at a given temperature, T, is given by $\chi = A_T/A$, where, A, is the total area of the exothermic peak between the temperature, T_i (crystallization is just beginning) and the temperature, T_f (the crystallization is completed) and, A_T, is the area between, T_i and T, as shown in Figure 11. The graphical representation of the crystallized volume fraction of the investigated glass samples at different heating rate shows typical sigmoid curve as a function of temperature in crystallization reactions which is widely discussed in the literatures [31-35]. The ratio between the ordinates of the DTA curve and the total area of the peak gives the corresponding crystallization rate, which makes it, is possible to build the curves of the exothermic peaks (Fig.

12). It is found that the values of, $(d\chi/dt)_p$, increase with increasing heating rate, which is a property that has been widely discussed in the literature [31, 32, 36]. From experimental values of, $(d\chi/dt)_p$, one can calculate the kinetic exponent, n, from the following equation [33-35];

$$(\mathbf{d\chi/dt})_\mathbf{p} = \mathbf{n(0.37\beta E_c)/(RT_p^2)} \quad (9)$$

The kinetic exponent, n, was deduced on the basis of the mechanism of crystallization [37]. The obtained values of the kinetic exponent, n, at 20 (K/min) heating rate (as an example) are listed in Table 3. The crystallization reaction mechanism of the $35P_2O_5$ $(45\text{-}x)V_2O_5$ xAs_2O_3 $20Fe_2O_3$ (x = 0, 10, 20 and 25 mol %) glass samples can be postulate from the average value of the kinetic exponent, n. Mahadevan et al. [26] shown that the kinetic exponent, n, may be 4, 3, 2 or 1, which are related to different glass-crystal transformation mechanism.

For n = 4, the growth kinetics is volume nucleation, three-dimensional growth; for n = 3, the growth kinetics is volume nucleation, two-dimensional growth; for n = 2, the growth kinetics is volume nucleation, one-dimensional growth; and for n = 1, the growth kinetics is surface nucleation, one-dimensional growth from surface to the inside. The kinetic exponent, n, of the investigated semiconducting glass samples for each of the experimental heating rates is found to be closed to 2 (n~2) this meaning that the growth kinetics of the semiconducting $35P_2O_5$ $(45\text{-}x)V_2O_5$ xAs_2O_3 $20Fe_2O_3$ (x = 0, 10, 20 and 25 mol %) glass samples is volume nucleation, one-dimensional growth.

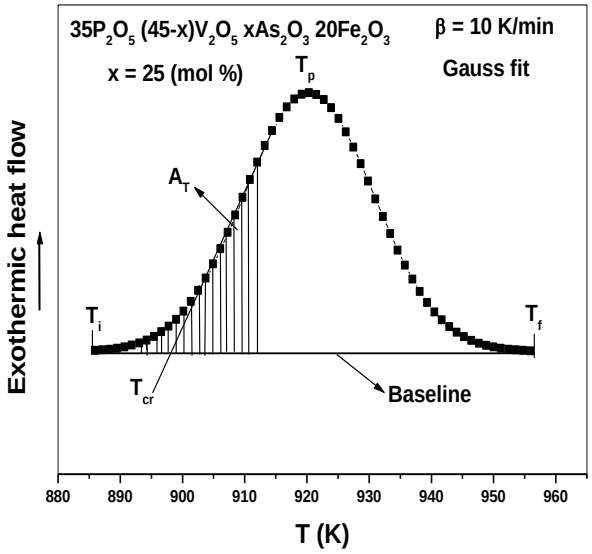

Fig. 11. DTA traces for $35P_2O_5$ $(45\text{-}x)V_2O_5$ xAs_2O_3 $20Fe_2O_3$ glass sample x = 25 (mol %) at 10 (K/min) heating rate; the lined area, A_T, shows between, T_i and T_f, of the peak. T_i, T_f, and, T, are according to the text.

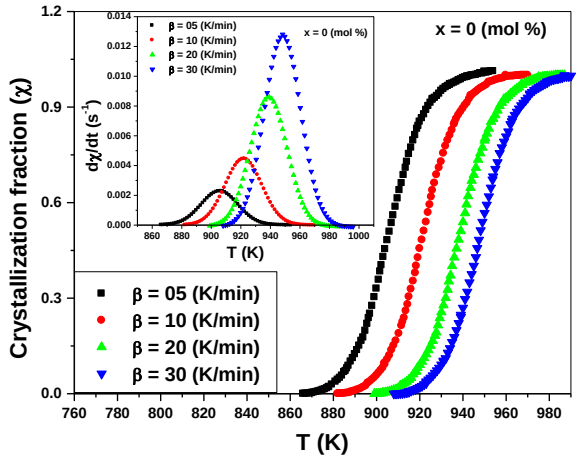

Fig. 12. Crystallized fraction, χ, as a function of temperature of the $35P_2O_5$ $(45\text{-}x)V_2O_5$ xAs_2O_3 $20Fe_2O_3$ glass sample x = 0 (mol %) at different heating rate. The inset shows crystallization rate vs. temperature of the glass sample x = 0 (mol %) at different heating rate.

To confirm the last results for the crystallization activation energy, E_c, which calculated from eq. (6) and Avrami exponent, n, which calculated from eq. (9) the next approach applied by Matusita et al. [38]. This approach state that for non-isothermal crystallization process the volume fraction of crystallites, χ, precipitated at a given temperature, T, in a glass heated at constant rate, β, can be related to the activation energy of crystallization, E_c, and to the Avrami exponent, n, through the following expression;

$$\ln[-\ln(1-\chi)] = -n\ln(\beta) - 1.052m\left(\frac{E_c}{RT}\right) + \text{const} \quad (10)$$

where, n, is the Avrami exponent depending on the nucleation process and, m, is an integer which depends on the dimensionality of the crystal. Where n = m + 1 is taken for as quenched glass containing no nuclei and n = m for a preheated glass containing sufficiently large number of nuclei [39, 40].

Fig. 13 shows the plots of $\ln[-\ln(1-\chi)]$ vs. $\ln(\beta)$ at four fixed temperatures for the $35P_2O_5$ $(45\text{-}x)V_2O_5$ xAs_2O_3 $20Fe_2O_3$ (x = 0 and 25 mol %) glass samples. The values of Avrami exponent, n, are determined from the slope of these curves at each temperature. It is found that the average values of Avrami exponent, n, are 1.805 and 2.26 for the glass samples with x = 0 and 25 (mol %) respectively. These results revealed that n, closed to 2 (n~2) and m = 1 this meaning that, the growth kinetics of the investigated glass samples with x = 0 and 25 (mol %) is volume nucleation, one-dimensional growth. Also it is found that the plot ln[-ln(1-χ)] vs. 1000/T [K^{-1}] is not straight line. This suggests that there is a variation in, E_c, and, n, during the crystallization process of glass [41, 42].

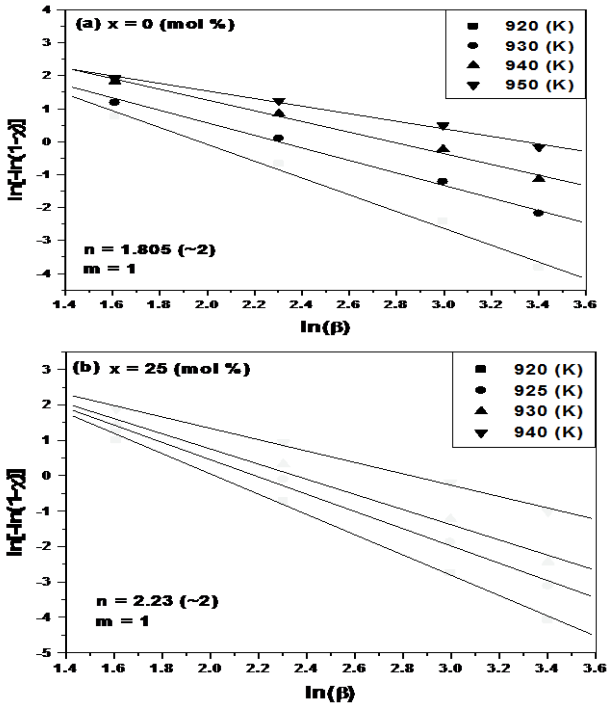

Fig. 13. Plots of ln[−ln(1− χ)] vs. ln(β) at different fixed temperatures for $35P_2O_5$ (45-x)V_2O_5 xAs_2O_3 20Fe_2O_3 glass samples with x = 0 and 25 (mol %).

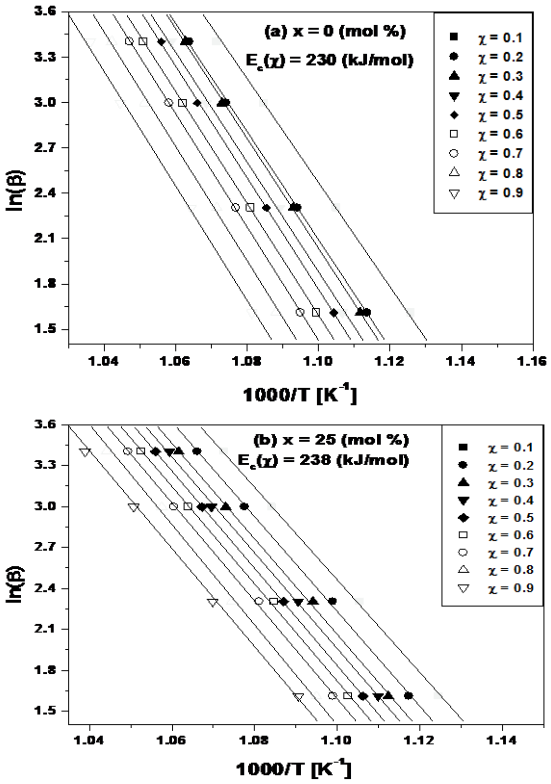

Fig. 14. Plots of ln(β) vs. 1000/T at various values of, χ, (0.1 < χ < 0.9) for $35P_2O_5$ (45-x)V_2O_5 xAs_2O_3 20Fe_2O_3 glass samples with x = 0 and 25 (mol %).

According to some previous articles the activation energy for different crystallization volume fractions is not constant in the whole transformation because of the change of nucleation and growth behaviors during the crystallization process [42]. The variation of the crystallization activation energy, E_c, and Avrami exponent, n, can be represented by the local activation energy, $E_c(\chi)$, and the local Avrami exponent, $n(\chi)$, [41, 43, 44].

From non-isothermal DTA results the local activation energy $E_c(\chi)$ is determined using the proposed method by Ozawa according to the following equation [45, 46];

$$\left[\frac{\mathbf{d(\ln(\beta))}}{\mathbf{d(1/T)}}\right]_{\chi} = -\frac{\mathbf{E_c(\chi)}}{\mathbf{R}} \qquad (\mathbf{11})$$

Fig. 14 shows the plots of ln(β) vs. 1000/T [K^{-1}] at various values of χ (0.1< χ <0.9) from the slope the local activation energies, $E_c(\chi)$, are calculated.

From the calculated values of the local activation energy for a non-isothermal crystallization process, $E_c(\chi)$, the local Avrami exponent, $n(\chi)$, is determined using the following equation [40, 41, 47];

$$\mathbf{n(\chi)} = -\frac{\mathbf{R}}{\mathbf{E_c(\chi)}}\left(\frac{\mathbf{\partial[\ln(-\ln(1-(\chi))]}}{\mathbf{\partial(1/T)}}\right) \qquad (\mathbf{12})$$

Fig. 15 shows the changes of, $E_c(\chi)$, and, $n(\chi)$, as a function of crystallization fraction, χ, at a heating rate of 10 (K/min) of the glass samples with x = 0 and 25 (mol %). For the glass samples with x = 0 and 25 (mol %) it is found that the local activation energies at the initial stage of crystallization process (χ = 0.1) are equal to 241 and 245 ± 3 (kJ/mol) which decrease slowly until 219 and 231 ± 3 (kJ/mol) for, χ = 0.9 respectively.

The mean values of, $E_c(\chi)$, for the glass samples with x = 0 and 25 (mol %) are 230 and 238 (kJ/mol) respectively. These results are in a good agreement with the results which calculated from Kissenger equation (eq. 6) for the crystallization activation energies, E_c, where the mean values are equal to 214.5 and 224.5 ± 3 (kJ/mol) for the glass samples with x = 0 and 25 (mol %) respectively.

Also it is found that the mean values of the local Avrami exponent, $n(\chi)$, of the investigated glass samples are 1.84 and 2.20 respectively which are closed to 2 and m = 1 (Fig. 15). The last results are in a good agreement with the average values of Avrami exponent $\langle n \rangle$ which are calculated from eq. (9) (Table 3) and eq. (10).

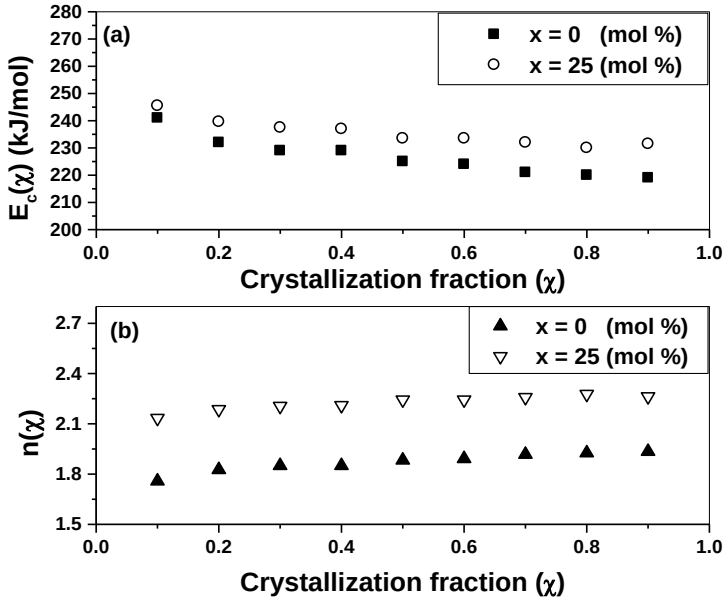

Fig. 15. (a) - Local activation energy for crystallization, $E_c(\chi)$, and (b) - Local Avrami exponent, $n(\chi)$, as a function of crystallization fraction, χ, at 10 (K/min) heating rate for $35P_2O_5$ (45-x)V_2O_5 xAs_2O_3 20Fe_2O_3 glass samples with x = 0 and 25 (mol %).

Table 1. Density, ρ, Molar volume, V_m, Dc conductivity, σ_{dc}, at different temperatures (303, 403 and 453 K) and activation energy, E_{dc}, of the $35P_2O_5$ (45-x)V_2O_5 xAs_2O_3 20Fe_2O_3 glass system.

As_2O_3 (mol %)	Density ρ (g/cm^3)	Molar volume V_m (cm^3/mol)	σ_{dc} (Scm^{-1}) 303 (K)	σ_{dc} (Scm^{-1}) 403 (K)	σ_{dc} (Scm^{-1}) 453 (K)	E_{dc} (eV) ± 0.011
0	2.96	55.27	1.14x10^{-5}	1.70x10^{-4}	4.17x10^{-4}	0.28
5	2.98	55.19	5.38x10^{-7}	2.67x10^{-5}	1.00x10^{-4}	0.41
10	3.01	55.03	2.83x10^{-7}	1.71x10^{-5}	6.94x10^{-5}	0.43
15	3.03	54.95	2.21x10^{-7}	1.54x10^{-5}	6.66x10^{-5}	0.45
20	3.04	54.82	4.46x10^{-8}	3.49x10^{-6}	1.48x10^{-5}	0.46
25	3.06	54.72	4.01x10^{-9}	4.30x10^{-7}	2.24x10^{-6}	0.49

Table 2. The values of thermal transition parameters; glass transition temperatures, T_{g1} and T_{g2}, onset temperature of crystallization, T_{cr}, crystallization peak temperature, T_p, and thermal stability criteria, ΔT_x, at 20 (K/min) heating rate and the values of A_{g1}, B_{g1}, A_{g2} and B_{g2} of $35P_2O_5$ (45-x)V_2O_5 xAs_2O_3 20Fe_2O_3 (x = 0, 10, 20 and 25 mol %) glass samples.

As_2O_3 (mol %)	T_{g1} (±2K)	T_{g2} (±2K)	T_{cr} (±2K)	T_p (±2K)	ΔT_x (±2K)	A_{g1} (±2K)	B_{g1}	A_{g2} (±2K)	B_{g2}
0	726	841	923	946	197	674.6	17.3	777.9	21.1
10	723	828	922	939	199	674.3	14.9	759.9	24.3
20	725	838	928	946	203	674.3	16.1	772.6	21.9
25	715	830	922	945	207	652.9	20.9	737.2	30.7

Table 3. The activation energies of glass transition, E_{g1}, E_{g2}, the crystallization activation energy, E_c, the pre-exp. factor, k_0, the maximum crystallization rate ($d\chi/dt$), and kinetic exponent, n, at 20 (K/min) and the average kinetic exponent $\langle n \rangle$ of $35P_2O_5$ (45-x)V_2O_5 xAs_2O_3 $20Fe_2O_3$ (x = 0, 10, 20 and 25 mol %) glass samples.

As_2O_3 (mol %)	E_{g1} (Kiss-Mah) (kJ/mol±3%)	E_{g2} (Kiss-Mah) (kJ/mol±3%)	E_c (kJ/mol±3%)	k_0 (S^{-1})	$(d\chi/dt)x10^{-3}$ (S^{-1})	n	$\langle n \rangle$
0	245 - 250	266 - 273	214.5	1.149E+14	9.451	1.934	1.929
10	280 - 281	296 - 298	219	1.149E+14	9.792	1.822	1.819
20	257 - 260	261 - 262	221	2.909E+14	9.858	1.907	1.905
25	196 - 199	174 - 181	224.5	2.547E+13	9.845	1.993	1.988

4 Conclusions

The effect of partial replacement of V_2O_5 by As_2O_3 on the density, molar volume, dc conductivity, thermal stability and crystallization kinetics of the semiconducting $35P_2O_5$ (45-x)V_2O_5 xAs_2O_3 $20Fe_2O_3$ glass system is studied in more details.

It is found that the density increases and the molar volume decreases with increasing As_2O_3 contents. The dc electrical conductivity decreases with decreasing V_2O_5 contents (TMO).

The electric conduction of the investigated amorphous semiconductor system dependent mainly on electron hopping from V^{4+} sites to the neighboring V^{5+} sites.

The thermal stability criteria, ΔT_x increases with increasing As_2O_3 contents this meaning that the partial replacement of V_2O_5 by As_2O_3 increases the thermal stability. The crystallization activation energy, E_c (nucleation barrier) is directly related to the width of the super-cooled liquid region, ΔT_x.

The kinetic exponent, n, of the investigated glass system is found to be closed to 2 (n~2) and m =1 this meaning that the growth kinetics of the investigated glass system is volume nucleation, one-dimensional growth

References

[1] J.J. Hudgens, R.K. Brow, D.R. Tallant, S.W. Martin, J. Non-Cryst. Solids 223 (1998) 21.

[2] C.G.S. Pillai, V. Sudarsan, M. Roy, A.K. Dua, J. Non-Cryst. Solids 321 (2003) 313.

[3] A. Chahine, M. Et-tabirou, J.L. Pascal, Mater. Lett. 58 (2004) 2776.

[4] A. Moguš-Milanković, A. Šantić, A. Gajović, D.E. Day, J. Non-Cryst. Solids 325 (2003) 76.

[5] S.T. Reis, D.L.A. Faria, J.R. Martinelli, W.M. Pontuschka, D.E. Day, C.S.M. Partini, J. Non-Cryst. Solids 304 (2002) 189.

[6] X. Yu, D.E. Day, G.J. Long, R.K. Brow, J Non-Cryst. Solids 215 (1997) 21.

[7] L. Baia, R. Stefan, W. Kiefer, J. Popp, S.J. Simon, J. Non-Cryst. Solids 303 (2002) 379.

[8] L. Montagne, G. Palavit, G. Mairesse, Phys. Chem. Glasses 37 (1996) 206.

[9] B. Santic, A. Mougs-Miliankovic, D.E. Day, J. Non-Cryst. Solids 296 (2001) 65.

[10] M. Shapaan, E.R. Shabaan, A.G. Mostafa, Physica B 404 (2009) 2058.

[11] M. Shapaan, J. Non-Cryst. Solids 356 (2010) 314.

[12] Dorina Rusu, I. Ardelean, Materials Research Bulletin 43 (2008) 1724.

[13] M. Shapaan, S.A. El-Badry, A.G. Mostafa, M.Y. Hassaan, M.H. Hazzaa, J. Phys. Chem. Solids 73 (2012) 407.

[14] A. Chahine, M. Et-tabirou, J.L. Pascal, Materials Letters 58 (2004) 2776.

[15] L. Murawski, C.H. Chung, J.D. Mackenize, J. Non-Cryst. Solids 32 (1979) 91.

[16] S. Sindhu, S. Sanghi, A. Agarwal, Sonam, V.P. Seth, N. Kishore, Physica B 365 (2005) 65.

[17] L. Murawski, R.J. Barczynski, Solid State Ionics 176 (2005) 2145.

[18] M.M. El-Desoky, M.Y. Hassaan, Phys. Chem. Glasses 43 (2002) 1.

[19] H. El-Mkami, B. Deroide, R. Backov, J.V. Zanchetto, J. Phys. Chem. Solids 61 (2000) 819.

[20] H.S. Chen, J. Non-Cryst. Solids 27 (1978) 257.

[21] M. Shapaan, J. Non-Cryst. Solids 355 (2009) 926.

[22] S. Muthupari, S. Prabakar, K.J. Rao, J. Phys. Chem. 98 (1994) 2646.

[23] Huaxin Li, Huixing Lin, Wei Chen, Lan Luo, J. Non-Cryst. Solids 352 (2006) 3069.

[24] M. Lasocka, Mater. Sci. Eng. A 23 (1976) 173.

[25] H.E. Kissinger, Anal. Chem. 29 (1957) 1702.

[26] S. Mahadevan, A. Giridhar, A.K. Singh, J. Non-Cryst. Solids 88 (1986) 11.

[27] J. Vazquez, P.L. Lopez-Alemany, P. Villares, R. Jimenez-Garay, J. Phys. Chem. Solids 61 (2000) 493.

[28] W. Johnson, R. Mehl, Trans. Am. Inst. Min. Met. Eng. 135 **(**1939) 416.

[29] M. Avrami, J. Chem. Phys. 8 (1940) 212.

[30] M. Avrami, J. Chem. Phys. 9 **(**1941) 177.

[31] R.A. Ligeno, J. Vazquex, M. Casns-Ruix, R. Jirnenez-Caray Thermochim. Acta 197 (1992) 319.

[32] C. Wagner, P. Villanes, J. Vazquex, R.R. Jirnenex-Caray, Mater. Lett. 19 **(**1993) 370.

[33] M. Shapaan, E.R. Shabaan, J. Phys. Chem. Solids 71 (2010) 1301.

[34] Essam R Shaaban, M. Shapaan, Yasser B Saddeek, J. Phys. Condens. Matter 20 (2008) 155108.

[35] Essam R. Shaaban, IshuKansal, M. Shapaan, J. Therm. Anal. Calorim. 98 (2009) 347.

[36] Gao Yi Qun, W. Wang, F.Q. Zheng, X. Liu, J. Non-Cryst. Solids 81 (1986) 135.

[37] K. Matusita, S. Saka, J. Non-Cryst. Solids 38 (1980) 741.

[38] K. Matusita, T. Komatsu, R. Yokota, J. Mater. Sci. 19 (1984) 291.

[39] Lamia Heireche, Mohamed Heireche, Maamar Belhadji, J. Crystallization Process and Technology 4 (2014) 111.

[40] Andreia A.S. Lopes, Roque S. Soares, Maria M.A. Lima, Regina C.C. Monteiro J. Applied Physics 115 (2014) 043516.

[41] W. Lu, B. Yan, W. Huang, J. Non-Cryst. Solids 351 (2005) 3320.

[42] A.A. Joraid, S. N. Alamri, A.A. Abu-Sehly, J. Non-Cryst. Solids 354 (2008) 3380.

[43] A. Calka, A.P. Radlinski, Mater. Sci. Eng. 97 (1988) 241.

[44] K. Lu, J.T. Wang, Mater. Sci. Eng. A 133 (1991) 500.

[45] T. Ozawa, J. Therm. Anal. 2 (1970) 301.

[46] T. Ozawa, J. Therm. Anal. 31 (1986) 547.

[47] K. Majhi, K. Varma, J. Mater. Sci. 44 (2009) 385.